PCCP

PAPER

View Article Online
View Journal | View Issue

Cite this: *Phys. Chem. Chem. Phys.*, 2016, **18**, 4476

A numerical model for charge transport and energy conversion of perovskite solar cells†

Yecheng Zhou and Angus Gray-Weale*

Received 9th September 2015,
Accepted 7th December 2015

DOI: 10.1039/c5cp05371d

www.rsc.org/pccp

Based on the continuity equations and Poisson's equation, we developed a numerical model for perovskite solar cells. Due to different working mechanisms, the model for perovskite solar cells differs from that of silicon solar cells and Dye Sensitized Solar Cells. The output voltage and current are calculated differently, and in a manner suited in particular to perovskite organohalides. We report a test of our equations against experiment with good agreement. Using this numerical model, it was found that performances of solar cells increase with charge carrier's lifetimes, mobilities and diffusion lengths. The open circuit voltage (V_{oc}) of a solar cell is dependent on light intensities, and charge carrier lifetimes. Diffusion length and light intensity determine the saturated current (J_{sc}). Additionally, three possible guidelines for the design and fabrication of perovskite solar cells are suggested by our calculations. Lastly, we argue that concentrator perovskite solar cells are promising.

Introduction

Perovskite was first induced to solar cells by Miyasaka *et al.* in 2009.[1] They rapidly developed, and Power Conversion Efficiencies (PCEs) reached 20%.[2–7] Excellent electron and hole diffusion ability[8,9] and very wide absorption wavelength range with high IPCE[10–12] of perovskite materials contribute to the solar cell's high performance. Theoreticians[13–18] are trying to find fundamental reasons for the performance, as experimentalist have done.[8,9,19,20] The structural and electronic properties of different phases of $CH_3NH_3PbI_3$ have been discussed.[14,18,21,22] They attribute the high performance to the low band gap and a large static dielectric constant. Frost *et al.* have suggested that transport along domain boundaries makes polarisation improve performance.[23,24] We studied the energy landscape of $CH_3NH_3PbI_3$ and found that polarisation makes a positive contribution through screening.[22] Although these theories have shown that perovskite materials have good electronic properties, it is still not fully understood how these properties affect light harvest and charge movement in its solar cells. To make this clear, numerical simulations are needed. Using the numerical model reported below, we can analyze how basic electronic parameters directly and quantitatively play roles in solar cells.

Theoretical simulations for silicon solar cells have developed for more than 40 years. In the late 1970s, computer-aided numerical analysis of silicon solar cells was developed by solving Poisson's equation and the hole and electron continuity equations.[25] The effect of interface states on high-performance amorphous silicon solar cells[26] and the effect of electrical mismatches in photovoltaic cell interconnection circuits have been discussed in detail.[27] The PC1D program was distributed by UNSW,[28,29] it is widely used for silicon solar cell analysis and optimization, such as modeling of free-carrier absorption,[29] enhancement of optical absorption,[30] wafer thickness optimization[31] and optimization of the device structure.[32] Numerical models for Dye Sensitized Solar Cells (DSSCs) and Bulk Heterojunction (BHJ) organic solar cells are also developed.[33–41] With these numerical methods, details of charge movement in solar cells and how a factor affects solar cell performance are revealed.

But these models for silicon solar cells and DSSCs are unable to describe the mechanism in perovskite solar cells (PSCs). The model developed for silicon solar cells is based on doping that forms a p–n junction. Dopant density and its distribution determine solar cell's performance, especially the output voltage.[41] The model for DSSCs involves solvent, which conducts ions and current. Additionally, its output voltage depends on the redox level in electrolytes.[38] For PSCs, the output voltage is dependent on the electron and hole quasi Fermi energy levels at corresponding electrodes, with no relation to dopants nor the redox level. Hence, the model should be adapted to PSCs. In PSCs, charge carriers are photon-generated holes and electrons, no ion migration contributes to current. The applied voltage is determined by the difference of quasi-Fermi energy levels at perovskite's two sides.

Numerical simulation of PSCs grows recently. Liu *et al.* using a general solar cell simulation program – AMPS-1D, show PSC's PCE dependence on thickness, defect density and charge mobility of its perovskite layer.[42] As we have discussed, a general model is unable

School of Chemistry, The University of Melbourne, Parkville, VIC, 3010, Australia. E-mail: gusgw@gusgw.net

† Electronic supplementary information (ESI) available. See DOI: 10.1039/c5cp05371d

to describe the charge transport behavior and mechanism in PSCs exactly. Assuming the electric field in the whole solar cell is constant and using general equations, Sun *et al.* get an analytical solution.[43] But their assumption contradicts the fact that the electric field in a real solar cell can never be constant. Additionally, though they get analytic solutions, parameters they used are obtained from the fitting of experimental *I–V* curves, which is more about fitting rather than prediction. Foster *et al.* developed a numerical model with specific parameters and physics for PSCs.[44] It is perhaps the best model to date, but it is costlier. Not only are many parameters unable to be obtained from experiment directly, but also they meet the difficulty of solving their equations with physically realistic parameter values. Reenen *et al.* proposed a model to explain the hysteresis in PSCs based on time evolution.[45] Although they could explain the hysteresis, their results are in poor agreement with quantitative measurements in Tress' experiments.[46] Here, we are going to introduce a new model for PSCs. Most of our equations are the same with Foster's models, but non-uniform generation and more recombination mechanisms are implemented in our model. Most importantly, there is not any problem with solving our equations with physically realistic parameter values.

In this paper, we started from basic semiconductor physics and build up a numerical solar cell model for PSCs. We first describe our equations and methods. Details are given in the Methods section and in the ESI.† Using this model, we studied PSC performance dependencies of various factors, such as light intensity, charge carrier's lifetime and mobility, to their performance including V_{oc}, J_{sc} and PCEs. These dependencies give us guidelines on how to design and optimize PSCs.

Methods

Semiconductor physics in PSCs

In PSCs, charge carriers include electrons and holes. Both of their diffusion and their drift contribute to output current. For hole transport, if hole density is p, the current induced by holes is:

$$J_p = J_{diffusion} + J_{drift} = -eD_p\frac{\partial p}{\partial x} + ep\mu_p F \quad (1)$$

where e is the elementary charge, F is the electric field and D_p is the hole diffusion coefficient. μ_p is hole mobility. In this work, we estimate mobilities from diffusion coefficients by using the Einstein relation $\left(\mu = \frac{eD}{kT}\right)$. For electron transport, we have

$$J_n = eD_n\frac{\partial n}{\partial x} + en\mu_n F \quad (2)$$

where n is electron density. D_n is the diffusion coefficient of electron. In our paper, 0.017 $cm^2\ s^{-1}$ and 0.011 $cm^2\ s^{-1}$ for D_n and D_p are used, which come from Stranks' experiment.[9] There are even larger values observed in experiment, such as 0.036 $cm^2\ s^{-1}$ and 0.022 $cm^2\ s^{-1}$.[8] For mobility dependence calculation, D_n and D_p are set at certain times higher than 0.017 $cm^2\ s^{-1}$ and 0.011 $cm^2\ s^{-1}$.

Conservation of charge carriers leads to continuity equation:

$$e\frac{\partial n}{\partial t} = \frac{\partial J_n}{\partial x} + eG - eR \quad (3)$$

For a steady state, charge density is constant: $\partial n/\partial t = 0$. Therefore, we have:

$$\frac{\partial J_n}{\partial x} = -eG + eR \quad (4)$$

$$\frac{\partial J_p}{\partial x} = eG - eR \quad (5)$$

where G and R are the generation rate and recombination rate, respectively. The electric field is solved by Poisson's equation,

$$\frac{\partial F}{\partial x} = e\frac{p-n}{\varepsilon\varepsilon_0} \quad (6)$$

Generally, we have five equations: eqn (1), (2) and (4)–(6). These five equations are used to solve five parameters: n, p, J_p, J_n and F. As all of these equations are first order differential, five boundary conditions are needed. At the photon-anode, $x = 0$, TiO_2 layer side, only electron can get out, therefore $J_p|_{x=0} = 0$. For the same reason, we have $J_n|_{x=d} = 0$ for photon-cathode. Then, the current boundary conditions are,

$$J_n|_{x=d} = 0$$
$$J_p|_{x=0} = 0 \quad (7)$$

Other boundary conditions are electric field strengths at two boundaries and the applied voltage between two boundaries.

$$F_{x=0} = F_0$$
$$F_{x=d} = F_d \quad (8)$$

A built-in electric field reduces the overall electric field within dielectric itself, when a dielectric matter is placed in an external field. A screening field is built up by capacitive charges, such as charged defects and charge in traps. It is hard to determine the specific boundary field due to the presence of TiO_2 and Spiro-OMeTAD layers and interface states. There are two extreme cases. One extreme case is that the built-in and screening field is stronger enough, $F_0 = F_d = 0$. Another extreme case is that there is no built-in and screening field at all, $F_0 = F_d = V/d$, if the field in perovskite is uniformly distributed. For a real solar cell, boundary fields should be between zero and V/d. In this paper, without specific notation, the field boundary conditions are $F_0 = F_d = V/d$. For more complex situations, we will discuss it elsewhere.

The output voltage of a PSC is the potential difference between the electron quasi-Fermi level at $x = 0$ and the hole quasi-Fermi level at $x = d$. $V = E_{fn}|_{x=0} - E_{fp}|_{x=d}$ (Fig. 1), where these Fermi levels satisfy: $n|_{x=0} = N_c e^{\frac{E_c - E_{fn}}{-kT}}$ and $p|_{x=d} = N_v e^{\frac{E_v - E_{fp}}{kT}}$, where N_c and N_v are the DOS of the conduction band and the

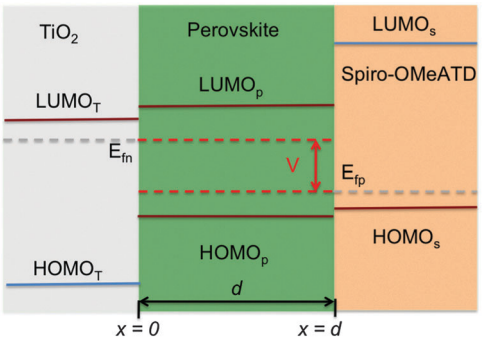

Fig. 1 Energy levels of TiO_2/$MAPbI_3$/Spiro-MeOTAD solar cells. The output voltage of a solar cell is the potential difference between the electron quasi-Fermi level at $x = 0$ and the hole quasi-Fermi level at $x = d$. $V = E_{fn}|_{x=0} - E_{fp}|_{x=d}$. The electron quasi-Fermi level in the TiO_2 layer is the same with it in the perovskite layer. The hole quasi-Fermi level in the Spiro-OMeATD layer is the same with it in the perovskite layer.

valence band, respectively. Hence, the applied voltage can be expressed as:

$$V = E_{fn} - E_{fp} = E_c + kT\ln\left(\frac{n|_{x=0}}{N_c}\right) - \left(E_v - kT\ln\left(\frac{p|_{x=d}}{N_v}\right)\right) = E_{bgap} + kT\ln\left(\frac{n|_{x=0}}{N_c}\right) + kT\ln\left(\frac{p|_{x=d}}{N_v}\right) \quad (9)$$

For an intrinsic semiconductor, its Fermi level locates at the center of conduction and valence bands. It requires $N_c = N_v$ to keep the semiconductor neutral. In our simulation, $N_c = N_v = 3.97 \times 10^{18}$ cm^{-3}, which is estimated from DFT calculation.[22] Therefore, the applied voltage is implemented as charge density at two boundaries:

$$n|_{x=0}p|_{x=d} = N_c N_v e^{\frac{E_{bgap}-V}{-kT}} \quad (10)$$

With these five equations and five boundary conditions, the solution is determined.

Generation rate and the recombination rate

The first process in solar cells is photon absorption–exciton formation–exciton separation. We name this process as photon-induced charge carrier generation, which can be expressed as G = IPCE × I_0, where IPCE is the Incident Photon-to-Current Efficiency and I_0 is the light incident density. Incident density decreases as photons go through medium. The generation rate is a function of depth (x) from the surface:

$$G(x) = \int_0^{\lambda_0} G(\lambda, x)\mathrm{d}\lambda = \int_0^{\lambda_0} \mathrm{IPCE}(\lambda) \times I(\lambda) \times \alpha(\lambda) \times e^{-\alpha(\lambda)x}\mathrm{d}\lambda \quad (11)$$

where λ is the wave length and λ_0 is the absorption edge. α is the absorption coefficient, which is 5.7×10^4 cm^{-1} for $\lambda = 500$ nm.[8] Here, we assume α is 5.7×10^4 cm^{-1} for photons with wavelength shorter than λ_0. For good PSCs, IPCEs for photons with wavelength shorter than λ_0 are higher than 80%.[4,10,47,48]

It is worth noticing the IPCE difference between experiment and eqn (11). In the calculation of experiment $\mathrm{IPCE}(\lambda) = \frac{\text{Current}}{\text{Incident light density}(\lambda)}$, which counts unabsorbed photons in. The relation between experiment and our IPCE is $\mathrm{IPCE}(\lambda)_{exp} = \mathrm{IPCE}(\lambda)_{theory} \times \int_0^d \alpha(\lambda)e^{-\alpha(\lambda)x}\mathrm{d}x < \mathrm{IPCE}(\lambda)_{theory}$. Without an infinite thickness perovskite layer, IPCE in theory should be higher than experimental IPCE. Hence, it is reasonable to set theoretical IPCE(λ) = 100% based on the experimental value of 80%. This assumption means all of the absorbed photons are transferred into charges.

The experiment band gap of $MAPbI_3$ differs with different experiments, it is in the region from 1.45 eV to 1.70 eV.[6,11,49–52] To have a direct comparison with Zhou's experiment I–V curve, a band gap of 1.55 eV from Zhou's experiment is used.[6] $I(\lambda)$ is calculated from the AM 1.5 spectrum provided by NREL.

When charges move, electrons and holes attract each other and try to combine. Recombination of free charge carriers in materials with low defect concentration and low mobility is often described with direct recombination. According to Langevin theory, the charge recombination rate is proportional to densities of electron and hole:[44,53,54]

$$R = r \times (n \times p - n_i^2) \quad (12)$$

r is the recombination coefficient and $n_i = N_c \times \exp\left(\frac{-E_{gap}}{2kT}\right)$ is the intrinsic carrier concentration. As big band gaps are present in perovskite materials, the intrinsic charge carrier is very small compared to photon generated charge carriers. Recombination also could happen through traps and defects, which can be described by the Shockley–Read–Hall (SRH) theory:[41,55,56]

$$R = \frac{np - n_i^2}{\tau_p(n + n_1) + \tau_n(p + p_1)} \quad (13)$$

τ_p and τ_n are lifetimes for the hole and the electron, respectively. While, n_1 and p_1 are dependent on the energy levels of the recombination centers: $n_1 = N_c \exp[-(E_C - E_d)/(kT)]$ and $p_1 = N_v \exp[(E_V - E_d)/(kT)]$. They are equilibrium electron and hole concentrations in a sample whose Fermi level coincides with the position of recombination centers. Due to its large band gap ($np \gg n_i^2$) and benign defects ($n_1 \ll n, p_1 \ll p$), eqn (13) goes to:

$$R = \frac{n \times p}{\tau_p n + \tau_n p} \quad (14)$$

which is also used in DSSC modelling.[35,38] In our model, we assume that lifetimes of the hole and electron are the same due to limited experiment values.

Methods to solve partial differential equations

The numerical solution is carried out by our own *Fortran* code. The shooting method with classical Runge–Kutta method was tried at first. A large amount of attempts are needed due to the charge density ranging from 10^{10} cm^{-3} to 10^{18} cm^{-3}. It is very time-consuming to shoot a solution in such a wide range. The specific method we used here is the method recommended for 'Two Point Boundary Value Problems' in *Numerical Recipes in Fortran*.[57]

As charge carrier's density varies in several magnitudes, the array *scalv* in our method is set as a variable rather than a constant as shown in *Numerical Recipes*. For more details, please refer to information provided in the ESI† and Chapter 17 in *Numerical Recipes in Fortran*.

Results

Comparison of two typical recombination mechanisms

There are two possible recombination mechanisms, one is direct recombination, which follows eqn (12); another is indirect recombination through defects, which follows the SRH model. Direct recombination happens in intrinsic bulk materials without defects, while indirect recombination happens at bulk defects or surfaces and interfaces. In Xing's experiment, lifetime is measured to be about 5 ns without a charge transport layer, it decreases to 0.37 ns and 0.64 ns by adding a PCBM or a Spiro-OMeTAD layer, respectively.[8] In Stranks' experiment, the thin film thickness is 180 nm, which is about three times thicker than Xing's (65 nm), carrier's lifetime increases to 9.6 ns. The presence of interface in their experiment also decreases its lifetime to 3.17 ns or 4.2 ns.[9] Improved methods usually give longer lifetime. For a modified two-step deposited 280 nm thickness $CH_3NH_3PbI_3$ film without or with infiltrated mesoporous TiO_2, the measured lifetimes are about 200 ns (without) and 6 ns (with).[58] All of these experiments suggest that the presence of interface decreases lifetime significantly, especially in a very thin film. These experiments imply interface recombination. Therefore, it is promising to refine interface states to increase PCEs. Zhou's work proves our guess.[6] They engaged with interface engineering and made solar cells with PCEs up to 19.3%, which is the highest record in all publications. In their experiment, a thin film deposed on the glass substrate shows a lifetime of about 382 ns and 736 ns. With this fact, the lifetime of intrinsic direct recombination should be about 736 ns. While the lifetime of interface recombination should be in the range of 0.1–10 ns, which is dependent on fabrication conditions, as shown in ref. 8, 9 and 58.

Here, we simulate the highest performance solar cell in ref. 6 with these two recombination mechanisms. The first model is implemented with the SRH mechanism. Its lifetime is set as 736 ns.[6] The second model, the recombination in solar cells is direct recombination, $R = rnp$. Parameters we used are shown in Table 1. Most of the parameters come from the experiment conducted by Zhou *et al.*[6] Diffusion coefficients are taken from Stranks' experiment.[9]

As shown in Table 2 and Fig. 2, J_{sc} are 22.93 mA cm^{-2} and 23.28 mA cm^{-2} for the SRH and direct recombination model, respectively. They are close to the experimental value of 22.75 mA cm^{-2}. The direct recombination model gives a larger filled factor (FF) as high as 79.89%. The FF of the SRH model is 76.15%, which is closer to FF (75.07%) in experiment. The most difference between experiment and simulation is V_{oc}. V_{oc} for the direct model is 1054 mV, varies away from the experimental value of 1130 mV. V_{oc} of the SRH model is 1153 mV, closer to experiment. Implementation of an interface region with 1 nm thickness and 6 ns lifetime gives better agreement on V_{oc}. Hence, we know that the performance reproduced by the SRH model is more accurate than the direct recombination model compared to experiment. The FF of the direct recombination model is a larger than that of the model with charge combined through defects. This indicates defects in thin film may lead to low FF. Charge densities, current densities and electric field in these simulated PSCs are shown in Fig. S3 in the ESI.†

From these simulations, we draw two conclusions. The first conclusion is that the SRH model is better than the direct recombination model to describe the recombination in PSCs. This conclusion indicates that most recombination in perovskite happens through defects rather than direct intrinsic recombination. Together with the fact that defects in the bulk of $CH_3NH_3PbI_3$ perovskite are benign,[21] this conclusion suggests that the recombination of charge carriers might mainly happen at domain surfaces and interfaces. This suggestion is verified by experiments that the lifetime of perovskite without an interface is much higher than that of perovskite film with an interface.[6,8,9,58] The second conclusion is that in a real PSC, the interface region with shorter charge carrier's lifetime is confirmed. This interface recombination leads to low V_{oc}. For this sake, a PSC with high J_{sc} and FF and low V_{oc} can be further improved by interface engineering. It is the key reason for Zhou *et al.* achieving a high V_{oc}.[6]

Charge carrier's lifetime dependence

Higher charge collection efficiencies and PCEs are expected with longer charge carrier lifetimes. This expectation is confirmed by our simulation results in Fig. 3. PCEs increase with carrier lifetime. Without an interface recombination, V_{oc} shows a certain relation with lifetime:

Table 1 Parameters used to simulate solar cells

Symbol	Meaning	Value	Symbol	Meaning	Value
d	Perovskite thickness	350 nm[6]	T	Temperature	300 K
N_c, N_v	Density of states	3.97×10^{18} cm^{-3}.[22]	I_l	Light intensity	1.5 AM
α	Absorption coefficient	5.7×10^4 cm^{-1}.[8]	IPCE	IPCE	100%
D_n	Electron diffusion coefficient	0.017 cm^2 s^{-1}.[9]	F_0, F_d	Boundary field	V/d
D_p	Hole diffusion coefficient	0.011 cm^2 s^{-1}.[9]	E_{bgap}	Band gap	1.55 eV[6]
r	Recombination coefficient	1.03×10^{-9} cm^3 s^{-1} [a]	τ	Lifetime	736 ns[6]
τ_{intf}	Lifetime for interface	6 ns			

[a] For direct recombination. The recombination coefficient (r) is estimated by fitting the experimental photoluminescence decay, more details are available in the ESI.

Table 2 Comparison of experiment performance and various simulation models

Source	V_{oc} (mV)	J_{sc} (mA)	PCEs (%)	FF
Direct recombination	1054	23.28	19.61	0.7989
SRH model without interface	1153	22.93	20.12	0.7615
SRH model with interface	1130	22.90	20.03	0.7743
Experiment[6]	1130	22.75	19.30	0.7507

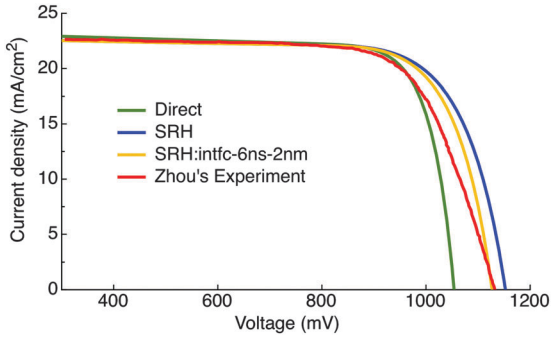

Fig. 2 Comparison of experiment with direct recombination model and SRH models. Red line is the experiment performance;[6] direct recombination model result is noted as green line; the result of the SRH model without interface recombination is shown in blue; the result of the SRH model with interface recombination is shown in yellow. The thickness of interface is 1 nm. Parameters are listed in Table 1.

$$V_{oc}\,(\mathrm{mV}) = A \times \ln(\tau - \tau_0) + V_0 \qquad (15)$$

for the results calculated with boundary conditions of $F_0 = F_d = 0$, V_0 is 900.1 mV, $\tau_0 = 0.209$ ns and $A = 52.354$ mV, which agrees well with approximated analytical models ($2kT$ = 52 meV) for DSSCs.[59–61] If we use diffusion coefficients with 0.034 cm^2 s^{-1} and 0.022 cm^2 s^{-1}, parameters change very little: V_0 = 902.902 mV, A = 51.810 mV. While for simulation results with boundary conditions of $F_0 = F_d = V/d$, V_0 = 622.286 mV, τ_0 = 3.635 ns and A = 80.633 mV, so A varies by $2kT$. Therefore, approximated analytical models are correct only when boundary fields are zero.

The presence of interface breaks this relation. No matter how many fitting parameters are, fitting curves vary away from simulation points, as shown in Fig. S7 in the ESI.† All of the V_0, J_{sc}, FF and PCEs increase with charge carrier lifetime no matter whether there is or not an interface. The V_{oc} difference between models with and without interface is 70 mV when carrier's lifetime is 700 ns, while J_{sc} difference is only 1 mA cm^{-2}. We also see that a thin interface decreases V_{oc} more than J_{sc} for a solar cell with a long diffusion length. I–V curves of these simulations are available in the ESI,† Fig. S8 and S9.

Mobility dependence

It is well known that a solar cell with high charge carrier mobilities should have high charge collection efficiency and large current. Here, we made a set of simulations with series mobilities. If the charge carrier's lifetime is set at 736 ns, performance is almost constant when mobilities change. This is because the diffusion length is longer than cell's thickness. Therefore, we set the lifetime as 20 ns for mobility dependence calculation. Mobilities were multiplied on mobilities of 0.65 and 0.42 cm^2 V^{-1} s^{-1}, which are calculated from diffusion coefficients of 0.017 cm^2 s^{-1} (electron) and 0.011 cm^2 s^{-1} (hole). As shown in Fig. S10 (ESI†), there is not much difference between performances of models with and without interfaces. This is because we set a short charge carrier's lifetime and a very thin interface region. V_{oc} differences among these simulations are within 4 mV, relative differences are within 0.5%. Therefore, mobilities are not reckoned as a factor affecting V_{oc}, while they change J_{sc} and PCEs very much. J_{sc} is improved from

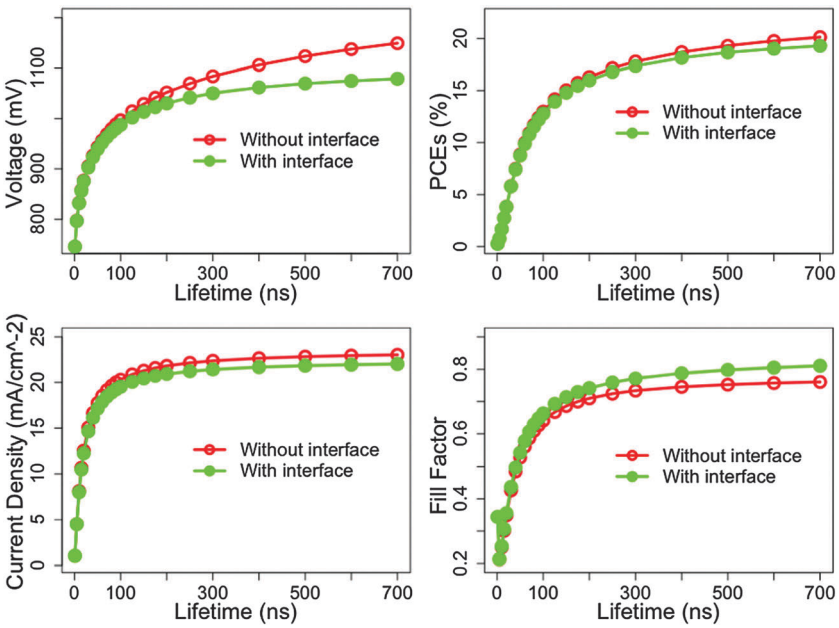

Fig. 3 Solar cells' performances with different charge carrier lifetimes from 1 ns to 700 ns. Other parameters are shown in Table 1.

12.6 mA cm^{-2} to 23.3 mA cm^{-2} and PCEs are improved from 3.8% to 14.5%, if mobilities increase from 0.65 and 0.42 cm^2 V^{-1} s^{-1} to 13.08 (electron) and 8.46 (hole) cm^2 V^{-1} s^{-1}. Both J_{sc} and PCEs increase a lot with mobilities increasing if the diffusion length $\left(L = \sqrt{D \times \tau}\right)$ is shorter than the length 3 times of solar cell's thickness. When the diffusion length is 3 times longer than the solar cell's thickness, further increasing of mobility gives little improvement.

Diffusion length dependence

The diffusion length is one important parameter of solar cells. It represents the overall charge transport character of a semiconductor. It is determined by charge carrier's lifetime and diffusion coefficient: $L_e = \sqrt{D_e \times \tau_e}$. Fig. 4 shows performances of solar cells with various D_e and D_h, while the diffusion length is fixed. In these simulations, τ decreases in order to keep the diffusion length constant. The diffusion lengths are 1.12 μm and 900 nm for the electron and hole, respectively. V_{oc} and PCEs decrease as D_e increases due to τ decreasing. J_{sc} has not much change, especially for the results of a solar cell without interfaces. Almost constant J_{sc} suggests that J_{sc} is only determined by carrier's diffusion length. With the diffusion length increasing (diffusion coefficient or lifetime increasing), J_{sc} increases very fast at the beginning, as shown in Fig. S10 in the ESI.† It almost reaches a saturated value of 23.3 mA cm^{-2} when the diffusion length is about 1.7 μm, which is about 5 times thicker than the perovskite layer thickness.

Light intensity dependence

The toxicity of lead compound limits the wide usage of PSCs. To avoid pollution, additional packaging is needed to seal whole solar cells. For large-scale solar cell fabrication, large packing area increases its cost significantly. The inner active part of a concentrator solar cell is much smaller than that of the normal one, this will save lots of packaging materials. Not only does it decreases the usage of perovskite, but also of the packaging materials. Hence, concentrator solar cells are very promising to reduce cost. Another motivation of concentrator solar cells is that they usually have higher PCEs than that of non-concentrated solar cells. For example, according to the data provided by NREL,[7] the record of single junction crystal GaAs solar cells is 26.4%, while, the record for its concentrator solar cell is 29.1%, about 10 percentage is improved. Here, we discuss the possibility of making concentrator PSCs. Various light intensities are implemented in simulations. J_{sc} is almost proportional to the light intensity. Normalized J_{sc} per Sun light intensity keep constant or change very little. As shown in Fig. 5, when light intensities increase from 1 to 1000 Sun light intensity, the normalized J_{sc} increase slightly from 23.07 mA cm^{-2} to 23.19 mA cm^{-2} for models without interface, from 22.06 mA cm^{-2} to 22.49 mA cm^{-2} for models with interface. It is the same with other types of solar cells, high light intensity increases V_{oc}.[62,63] Without interface, V_{oc} increases from 1153 mV to 1542 mV for irradiation intensity increasing from 1 to 600 Sun. The constant normalized J_{sc} and increasing V_{oc} with light intensity are in good agreement with the experiment.[64] For 700 Sun irradiation, V_{oc} is larger than its band gap of 1.55 eV. This is due to the photon generated charge carrier concentration being higher than the DOS of perovskite, which never happens in a real case. Saturable absorption happens when light intensity becomes extreme. In this case, absorption does not increase with light increasing. FF increases from 81.3% to 86.7% (with interface) or from 76.2% to 85.6%

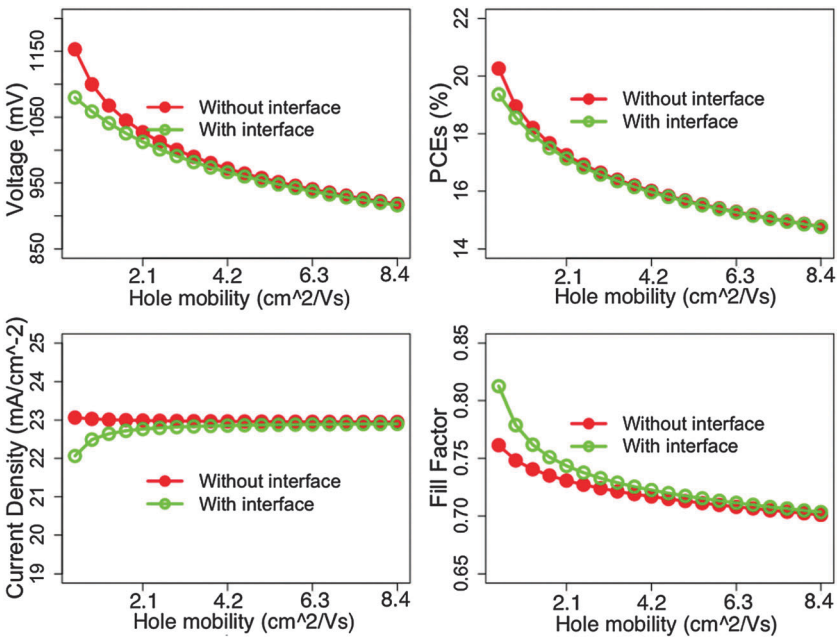

Fig. 4 Solar cells' performances with various mobilities and lifetimes. The diffusion lengths are kept as 1.12 μm and 900 nm for the electron and hole, respectively. Both of the electron and hole mobilities increase, while the lifetime decreases. The interface recombination width is 1 nm and its lifetime is 1 ns. Other parameters are listed in Table 1.

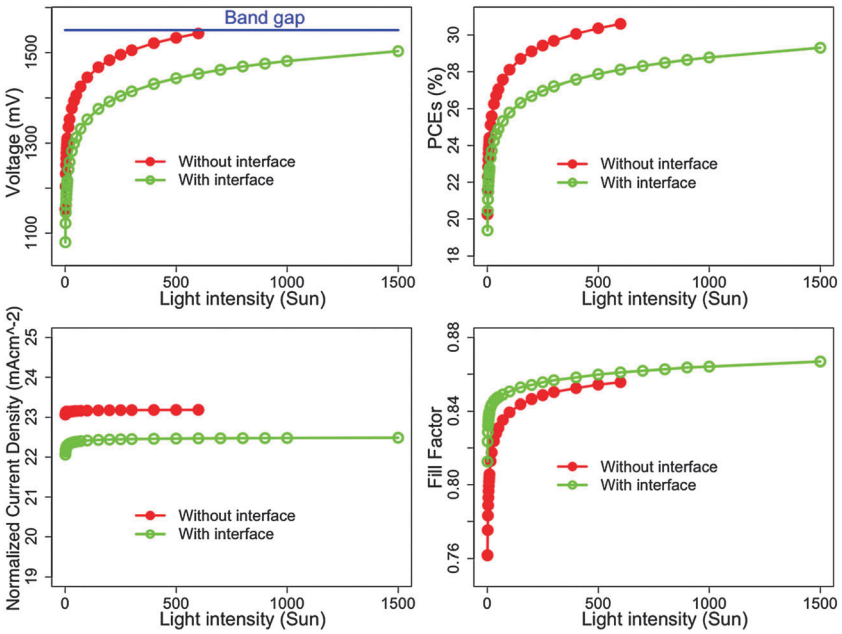

Fig. 5 Light intensity dependence. The interface recombination width is 1 nm and its lifetime is 1 ns. Other parameters are shown in Table 1.

(without interface). The most impressive is the improvement of PCEs, which increases from 20.3% to 30.6% for models without interface when light intensity increases from 1 to 600 Sun. For models with interface, it raises from 19.4% to 29.3%, when light intensity increases from 1 to 1000 Sun. Under high incident light intensity, high-density charge carriers are generated and transported to two ends of the perovskite layer, and then, higher V_{oc} and PCEs are expected.

In experiment, one junction GaAs cells showed a logarithmic relation for the efficiency and concentration, if the concentration is lower than 500 times.[65] This trend is in good agreement with our simulation result, as shown in Fig. 6. When the incident light becomes extremely intensive, PCE no longer increases and even decreases.[63,66] We reckon two reasons contribute to the difference at extreme light intensity. The first one is that the saturable absorption, which refers to light absorption does not increase with light intensity. The second reason is heat accumulation at high light intensity. Heat accumulation increases solar cell's temperature and then lowers it performance. For a solar cell with interface, it works at 300 K under 800 Sun, its PCE is 28.5%. It decreases to 27.6% when it works at 350 K, shown as a blue cycle in Fig. 6. For a solar cell working under 1000 Sun, its PCE decreases from 28.8% to 27.2% when the working temperature increases from 300 K to 400 K. For a solar cell working under 1500 Sun, its PCE decreases from 29.3% to 26.6% when the working temperature increases from 300 K to 500 K. There is another problem for heat accumulation: phase transition. The β phase $MAPbI_3$ will go to its α phase, when the temperature is above 330 K. Therefore, for the $MAPbI_3$ concentrator solar cells, the cooling system is very crucial (Fig. 6).

Temperature dependencies

We study temperature dependent performance in order to let solar cells work under optimum conditions and output at maximum. It is found that the temperature affects J_{sc} very little.

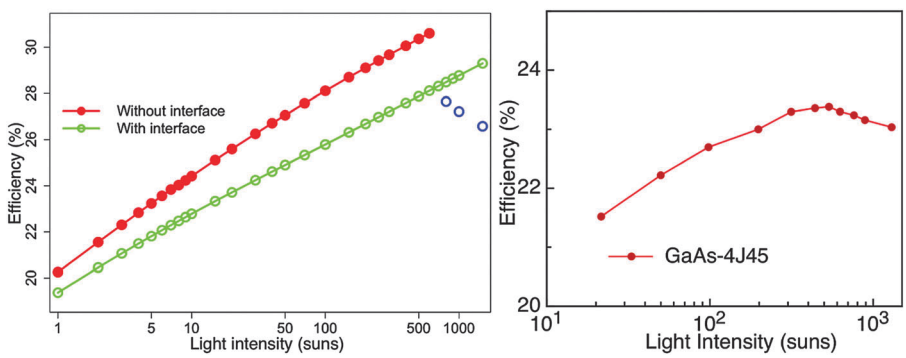

Fig. 6 Light intensity dependence tendency compared to experiment of GaAs solar cells. Left are simulation results, right are the results from experiment.[65] For simulation, the interface recombination width is 1 nm and its lifetime is 1 ns. PCEs of PSCs simulated under 300 K is shown in red or green. Blue points are the results simulated with a temperature of 350 K, 400 K and 500 K, from left to right, respectively. Other parameters are shown in Table 1.

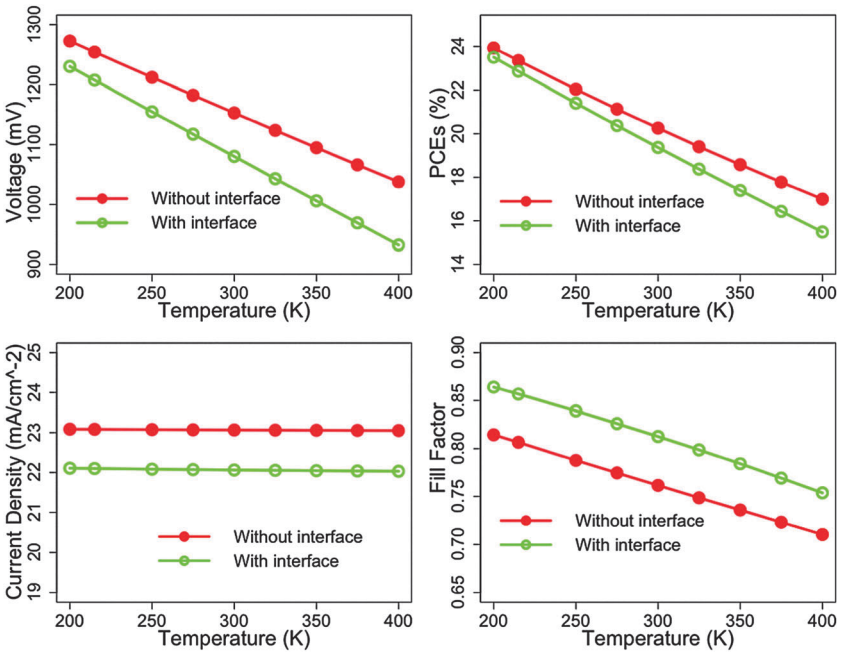

Fig. 7 Performances of PSCs at temperature from 200 to 400 K. The interface recombination width is 1 nm and its lifetime is 1 ns. Other parameters are shown in Table 1.

It decreases from 23.08 mA cm^{-2} to 23.05 mA cm^{-2}, when the temperature increases from 200 K to 400 K, as shown in Fig. 7. For solar cells with interface, J_{sc} drops from 22.11 mA cm^{-2} to 22.03 mA cm^{-2}. As we expected, V_{oc} decreases from 1272 meV to 1037 meV as temperature rises from 200 K to 400 K. From this simulation, we draw a conclusion that, without phase transition, PSCs working at lower temperature give higher PCEs.

A phase transition happens at 330.15 K, where $MAPbI_3$ goes from the β phase to the α phase. According to Landau–Ginzburg theory of fluctuations, the correlation length near the transition temperature (T_c) is proportional to $1/\sqrt{|T - T_c|}$. Long correlation length gives high mobility and long diffusion length. If we assume that, diffusion coefficients can be calculated by $D = \frac{D^0}{|T - T_c|}$. Considering diffusion coefficients for the electron and hole at 300 K are 0.017 and 0.011 $cm^2\ s^{-1}$, D^0 for electron and hole should be 0.51 and 0.33 $cm^2\ s^{-1}$, respectively. In this case, the highest performance is found at low temperature or near T_c. V_{oc} continuously decreases as temperature rises. FF and J_{sc} show a 'transition point' at T_c. J_{sc} increases with temperature increasing when its temperature is below T_c. It decreases when temperature is higher than T_c. The highest PCE in these simulations is 22.02%, which is at the lowest temperature. Below T_c, PCEs decrease at first and then increase when temperature is near T_c. It decreases again when temperature continues to rise. Actually, different devices show different performance dependence. For a PSC with very short diffusion length, the maximum PCE locates at 330 K, as shown Fig. S11 in the ESI.†

Thickness dependence

To design a high performance solar cell, a cell's thickness is one key parameter. Perovskite layers need to be thick in order to absorb more possible photons. On the other hand, a perovskite layer too thick makes it hard for the photon generated charge carriers to be transported out, which reduces its performance. An optimum thickness should be in a balance of its absorption length and diffusion length. For models with boundary conditions of $F_0 = F_d = 0$ and without interface recombination, solar cells with a lifetime of 100 ns the optimum thickness is about 375 nm, shown in Fig. 8. If the lifetime increased to 300 ns, the optimum thickness is around 500 nm. For lifetimes of 700 ns, 1000 ns and 1500 ns, the optimum thicknesses are 600 nm, 650 nm and 700 nm, respectively. When we model it with interfaces, shown in Fig. S12 (ESI†), the optimum thickness are 375 nm, 500 nm, 550 nm, 550 nm and 600 nm for lifetimes of 100 ns, 300 ns, 700 ns, 1000 ns and 1500 ns. Based on these trends, we draw a conclusion that the upper limit of the

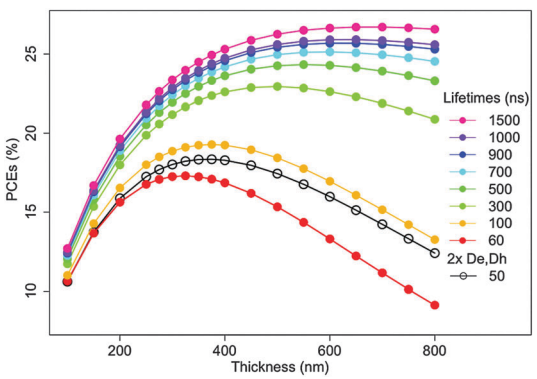

Fig. 8 The thickness dependent PCEs. The optimum thickness is dependent on the diffusion length. Simulated with boundary fields $F_0 = F_d = 0$. The results with boundary fields $F_0 = F_d = V/D$ are shown in the ESI.† Lifetime changed in order to change the diffusion length. Other parameters are listed in Table 1.

optimum perovskite layer thickness is 600 nm with interface recombination. For models with $F_0 = F_d = V/d$, the results are shown in Fig. S13 and S14 in the ESI.†

As shown in Fig. 8, the thickness dependence of the model with a lifetime of 100 ns and diffusion coefficients of 0.017 and 0.011 $cm^2\ s^{-1}$ is the same as that of the model with a lifetime of 50 ns and diffusion coefficients of 0.034 and 0.022 $cm^2\ s^{-1}$. This fact suggests that optimum thickness is solely dependent on the diffusion length. As the absorption coefficient of perovskite thin film is $5.7 \times 10^4\ cm^{-1}$, the absorption length is 175 nm. Shown in Fig. 8, when the diffusion length is shorter than the absorption length, the optimum length is about the diffusion length. For the diffusion length much longer than the absorption length, the optimum length is still similar to the absorption length.

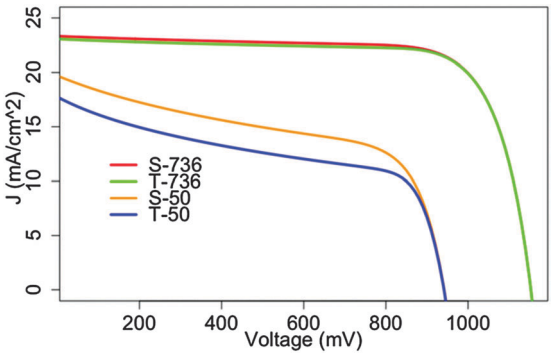

Fig. 9 Performances of solar cells with two types of structures and different lifetimes. Boundary fields are $F_{x=0} = F_{x=d} = V/d$. The results with boundary field $F_0 = F_d = 0$ are shown in the ESI.†

Discussion

Sunlight may enter the perovskite layer either through the TiO_2 layer or the Spiro-MeOTAD layer. The question is which structure is better to achieve high PCE solar cells? Due to large band gaps of TiO_2 and Spiro-MeOTAD, it is reasonable to neglect the absorption of these two layers. The model with light coming from the TiO_2 layer is noted as T model. The model with light coming from the Spiro-MeOTAD layer is noted as S model. The difference between them is where are the high density charge carriers generate. For the S model, light in perovskite near the Spiro-MeOTAD side is more intensive than that near the TiO_2 side. Hence, more charge carriers are generated near the Spiro-MeOTAD side. In this model, electrons need to travel a long distance from the Spiro-MeOTAD side to the TiO_2 side. In the T model, for the same reason, holes need to travel a long distance from the TiO_2 side to the Spiro-MeOTAD side. As electron's mobility is higher than hole's in $CH_3NH_3PbI_3$, it is easier for electron traveling a far distance. Therefore, the S model should show better performance than the T model could do.

Simulations give the same results as we analyzed. V_{oc} is nearly the same. What is different is J_{sc}. They are 23.07 mA cm^{-2} and 23.32 mA cm^{-2} for T and S models with a lifetime of 736 ns, respectively. PCEs are 20.25 and 20.30%, no much difference, which is due to its large diffusion length is much longer than perovskite layer's thickness. For a solar cell with shorter lifetime, these two structures show big difference. As shown in Fig. 9, the J_{sc} of solar cells with a lifetime of 50 ns are 19.70 mA cm^{-2} and 17.75 mA cm^{-2} for S and T models, respectively. Corresponding PCEs are 10.13% and 8.77%, more than 2% PCEs are improved if we use the S model. Models with interface and different boundary conditions show the same results. Details are provided in the ESI.† Generally, as the electron mobility is higher than hole's, it is better to fabricate cells with light coming from the Spiro-MeOTAD side.

As we have shown in Results, short diffusion length leads to low V_{oc} and small J_{sc}. For such a solar cell, increasing of charge carrier's mobility and lifetime improves its performance. Therefore, a cell with low V_{oc} and small J_{sc} can be improved by the engineering of perovskite thin film. When should we focus on the interface engineering? Fig. 2 and Fig. S7 in the ESI† show that the presence of a very thin interface changes J_{sc} little, but changes V_{oc} a lot. Therefore, for a cell with large J_{sc} and small V_{oc}, we should refine its interface states.

Conclusion

In this work, we built a numerical model with two different recombination mechanisms and methods. The model with SRH recombination is in better agreement with experiment than the model with direct recombination, which indicates that the recombination in hybrid PSCs is mainly through defects and traps. It is found that PCEs are determined by charge carrier's lifetimes, diffusion coefficients and diffusion lengths. J_{sc} is solely determined by charge carrier's diffusion lengths, and V_{oc} depends on the charge carrier's lifetime. The temperature dependencies are discussed based on two different assumptions. If the mobility is constant, performance decreases as temperature increases. Another assumption is that mobilities may change near the phase transition point. The correlation length near the transition temperature (T_c) is, we expect, proportional to $1/\sqrt{|T - T_c|}$. Long correlation length leads to high mobility and long diffusion length. Then, we expect to find the best performance near T_c or at the lowest accessible temperature. Lastly, simulations show that the presence of interface decreases V_{oc}, J_{sc} and PCEs.

We demonstrated how to use this model to provide guidelines for PSC design and optimization. First, for a material with electron mobility higher than hole mobility, the cell with the hole transport layer facing the sun has a higher PCE than the cell with the electron transport layer facing the sun. Second, the optimum thickness of the active layer is dependent on its absorption coefficient and its diffusion length. When the diffusion length is shorter than the absorption length, the optimum length is about the diffusion length. But for the diffusion length far longer than the absorption length, the optimum length is still in the magnitude of the absorption length. Third, a solar cell with a thin rapid interface recombination shows a low V_{oc} and high J_{sc}. It suggests that a solar cell with low V_{oc} and high J_{sc} can be improved by interface engineering. A solar cell with both low V_{oc} and low J_{sc} is mainly due to poor charge transport ability in

the perovskite layer. Enhancing the quality of perovskite thin film is crucial. Lastly, the light dependence of PSCs indicated perovskite concentrator solar cells are the possible new developing directions for PSCs.

These equations and methods we have reported and tested provide a framework for numerical modeling of perovskite-based cells and the optimization of their performance.

References

1 A. Kojima, K. Teshima, Y. Shirai and T. Miyasaka, *J. Am. Chem. Soc.*, 2009, **131**, 6050–6051.
2 P. Docampo, J. M. Ball, M. Darwich, G. E. Eperon and H. J. Snaith, *Nat. Commun.*, 2013, **4**, 2761.
3 G. Hodes, *Science*, 2013, **342**, 317–318.
4 M. M. Lee, J. Teuscher, T. Miyasaka, T. N. Murakami and H. J. Snaith, *Science*, 2012, **338**, 643–647.
5 M. Liu, M. B. Johnston and H. J. Snaith, *Nature*, 2013, **501**, 395–398.
6 H. Zhou, Q. Chen, G. Li, S. Luo, T.-b. Song, H.-S. Duan, Z. Hong, J. You, Y. Liu and Y. Yang, *Science*, 2014, **345**, 542–546.
7 National Renewable Energy Laboratory (NREL), Research Cell Efficiency Records, 2015, http://www.nrel.gov/ncpv/images/efficiency_chart.jpg.
8 G. Xing, N. Mathews, S. Sun, S. S. Lim, Y. M. Lam, M. Grätzel, S. Mhaisalkar and T. C. Sum, *Science*, 2013, **342**, 344–347.
9 S. D. Stranks, G. E. Eperon, G. Grancini, C. Menelaou, M. J. P. Alcocer, T. Leijtens, L. M. Herz, A. Petrozza and H. J. Snaith, *Science*, 2013, **342**, 341–344.
10 J. Burschka, N. Pellet, S.-J. Moon, R. Humphry-Baker, P. Gao, M. K. Nazeeruddin and M. Grätzel, *Nature*, 2013, **499**, 316–319.
11 H.-S. Kim, C.-R. Lee, J.-H. Im, K.-B. Lee, T. Moehl, A. Marchioro, S.-J. Moon, R. Humphry-Baker, J.-H. Yum, J. E. Moser, M. Grätzel and N.-G. Park, *Sci. Rep.*, 2012, **2**, 591.
12 Z. Ku, Y. Rong, M. Xu, T. Liu and H. Han, *Sci. Rep.*, 2013, **3**, 3132.
13 I. Borriello, G. Cantele and D. Ninno, *Phys. Rev. B: Condens. Matter Mater. Phys.*, 2008, **77**, 235214.
14 F. Brivio, A. B. Walker and A. Walsh, *APL Mater.*, 2013, **1**, 042111.
15 J. Even, L. Pedesseau, J.-M. Jancu and C. Katan, *J. Phys. Chem. Lett.*, 2013, **4**, 2999–3005.
16 J. Hong, A. Stroppa, J. Íñiguez, S. Picozzi and D. Vanderbilt, *Phys. Rev. B: Condens. Matter Mater. Phys.*, 2012, **85**, 054417.
17 P. Umari, E. Mosconi and F. De Angelis, *Sci. Rep.*, 2014, **4**, 4467.
18 Y. Wang, T. Gould, J. F. Dobson, H. Zhang, H. Yang, X. Yao and H. Zhao, *Phys. Chem. Chem. Phys.*, 2013, **16**, 1424–1429.
19 H. J. Snaith, *J. Phys. Chem. Lett.*, 2013, **4**, 3623–3630.
20 T. Baikie, Y. Fang, J. M. Kadro, M. Schreyer, F. Wei, S. G. Mhaisalkar, M. Graetzel and T. J. White, *J. Mater. Chem. A*, 2013, **1**, 5628.
21 M. H. Du, *J. Mater. Chem. A*, 2014, **2**, 9091.
22 Y. Zhou, F. Huang, Y.-B. Cheng and A. Gray-Weale, *Phys. Chem. Chem. Phys.*, 2015, **17**, 22604–22615.
23 J. M. Frost, K. T. Butler and A. Walsh, *APL Mater.*, 2014, **2**, 081506.
24 J. M. Frost, K. T. Butler, F. Brivio, C. H. Hendon, M. van Schilfgaarde and A. Walsh, *Nano Lett.*, 2014, **14**, 2584–2590.
25 J. G. Fossum, *Solid-State Electron.*, 1976, **19**, 269–277.
26 H. Tasaki, W. Y. Kim, M. Hallerdt, M. Konagai and K. Takahashi, *J. Appl. Phys.*, 1988, **63**, 550.
27 J. Bishop, *Sol. Cells*, 1988, **25**, 73–89.
28 P. Basore, *IEEE Trans. Electron Devices*, 1990, **37**, 337–343.
29 D. A. Clugston and P. A. Basore, *Prog. Photovolt.: Res. Appl.*, 1997, **5**, 229–236.
30 A. Nakajima, T. Suzuki, M. Yoshimi and K. Yamamoto, *Sol. Energy Mater. Sol. Cells*, 1997, **48**, 287–294.
31 C. Tool, P. Manshanden, A. Burgers and A. Weeber, *Sol. Energy Mater. Sol. Cells*, 2006, **90**, 3165–3173.
32 G. Dingemans and W. M. M. Kessels, *J. Vac. Sci. Technol., A*, 2012, **30**, 040802.
33 A. Usami, *Chem. Phys. Lett.*, 1998, **292**, 223–228.
34 J. a. Anta, F. Casanueva and G. Oskam, *J. Phys. Chem. B*, 2006, **110**, 5372–5378.
35 K. Ogiya, C. Lv, A. Suzuki, R. Sahnoun, M. Koyama, H. Tsuboi, N. Hatakeyama, A. Endou, H. Takaba, M. Kubo, C. A. Del Carpio and A. Miyamoto, *Jpn. J. Appl. Phys.*, 2008, **47**, 3010–3014.
36 J. a. Anta, *Energy Environ. Sci.*, 2009, **2**, 387.
37 J. Villanueva, J. A. Anta, E. Guillen and G. Oskam, *J. Phys. Chem. C*, 2009, **113**, 3–4.
38 M. Onodera, K. Ogiya, A. Suzuki, H. Tsuboi, N. Hatakeyama, A. Endou, H. Takaba, M. Kubo and A. Miyamoto, *Jpn. J. Appl. Phys.*, 2010, **49**, 04DP10.
39 J. Cai and L. Han, *J. Phys. Chem. C*, 2011, **115**, 17154–17162.
40 J. A. Anta, E. Guillén and R. Tena-Zaera, *J. Phys. Chem. C*, 2012, **116**, 11413–11425.
41 P. P. Altermatt, *J. Comput. Electron.*, 2011, **10**, 314–330.
42 F. Liu, J. Zhu, J. Wei, Y. Li, M. Lv, S. Yang, B. Zhang, J. Yao and S. Dai, *Appl. Phys. Lett.*, 2014, **104**, 253508.
43 X. Sun, R. Asadpour, W. Nie, A. D. Mohite and M. A. Alam, *IEEE J. Photovolt.*, 2015, **5**, 1389–1394.
44 J. M. Foster, H. J. Snaith, T. Leijtens and G. Richardson, *SIAM J. Appl. Math.*, 2014, **74**, 1935–1966.
45 S. van Reenen, M. Kemerink and H. J. Snaith, *J. Phys. Chem. Lett.*, 2015, 3808–3814.
46 W. Tress, N. Marinova, T. Moehl, S. M. Zakeeruddin, M. K. Nazeeruddin and M. Grätzel, *Energy Environ. Sci.*, 2015, **8**, 995.
47 F. Huang, *et al.*, *Nano Energy*, 2014, **10**, 10–18.
48 H. Zhang, X. Qiao, Y. Shen, T. Moehl, S. M. Zakeeruddin, M. Grätzel and M. Wang, *J. Mater. Chem. A*, 2015, **3**, 11762–11767.
49 W.-J. Yin, T. Shi and Y. Yan, *Adv. Mater.*, 2014, **26**, 4653–4658.
50 C. C. Stoumpos, C. D. Malliakas and M. G. Kanatzidis, *Inorg. Chem.*, 2013, **52**, 9019–9038.
51 Y. Yamada, T. Nakamura, M. Endo, A. Wakamiya and Y. Kanemitsu, *Appl. Phys. Express*, 2014, **7**, 032302.
52 P. Schulz, E. Edri, S. Kirmayer, G. Hodes, D. Cahen and A. Kahn, *Energy Environ. Sci.*, 2014, **7**, 1377.

53 D. J. Wehenkel, L. J. A. Koster, M. M. Wienk and R. a. J. Janssen, *Phys. Rev. B: Condens. Matter Mater. Phys.*, 2012, **85**, 1–12.
54 L. J. a. Koster, V. D. Mihailetchi, R. Ramaker and P. W. M. Blom, *Appl. Phys. Lett.*, 2005, **86**, 123509.
55 W. Shockley and W. Read, *Phys. Rev.*, 1952, **87**, 835–842.
56 R. Hall, *Phys. Rev.*, 1952, **87**, 387.
57 W. Press, S. Teukolsky, W. Vetterling and B. Flannery, *Numerical Recipes in FORTRAN; The Art of Scientific Computing*, Cambridge University Press, New York, 2nd edn, 1992.
58 J. Shi, Y. Luo, H. Wei, J. Luo, J. Dong, S. Lv, J. Xiao, Y. Xu, L. Zhu, X. Xu, H. Wu, D. Li and Q. Meng, *ACS Appl. Mater. Interfaces*, 2014, **6**, 9711–9718.
59 F. E. Gálvez, E. Kemppainen, H. Mguez and J. Halme, *J. Phys. Chem. C*, 2012, **116**, 11426–11433.
60 S. Soedergren, A. Hagfeldt, J. Olsson and S.-e. Lindquist, *J. Phys. Chem.*, 1994, **98**, 5552–5556.
61 J. Halme, P. Vahermaa, K. Miettunen and P. Lund, *Adv. Mater.*, 2010, **22**, E210–E234.
62 E. Guillén, L. M. Peter and J. A. Anta, *J. Phys. Chem. C*, 2011, **115**, 22622–22632.
63 R. Sinton, J. Gan and R. Swanson, *IEEE Electron Device Lett.*, 1986, **7**, 567–569.
64 D. Bi, L. Yang, G. Boschloo, A. Hagfeldt and E. M. J. Johansson, *J. Phys. Chem. Lett.*, 2013, **4**, 1532–1536.
65 M. Yamaguchi and A. Luque, *IEEE Trans. Electron Devices*, 1999, **46**, 2139–2144.
66 M. Yamaguchi, T. Takamoto and K. Araki, *Sol. Energy Mater. Sol. Cells*, 2006, **90**, 3068–3077.

